

Thermal properties and surface reactivity in simulated body fluid of new strontium ion-containing phosphate glasses

J. Massera · L. Petit · T. Cardinal ·
J. J. Videau · M. Hupa · L. Hupa

Received: 15 November 2012 / Accepted: 8 March 2013 / Published online: 20 March 2013
© Springer Science+Business Media New York 2013

Abstract In this paper, we investigate the effect of SrO substitution for CaO in $50\text{P}_2\text{O}_5-10\text{Na}_2-(40-x)\text{CaO}-x\text{SrO}$ glass system (x from 0 to 40) on the thermal and structural properties and also on the glass reactivity in simulated body fluid (SBF) in order to find new glass candidates for biomedical glass fibers. The addition of SrO at the expense of CaO seems to restrain the leaching of phosphate ions in the solution limiting the reduction of the solution pH. We observed the formation of an apatite layer at the surface of the glasses when in contact with SBF. SrO and MgO were found in the apatite layer of the strontium ion-containing glasses, the concentration of which increases with an increase of SrO content. We think that it is the presence of MgO and SrO in the layer which limits the leaching of phosphate in the solution and thus the glass dissolution in SBF.

1 Introduction

Demand for biomedical glass fibers has increased in the past decade. Fibers based on bioactive glasses can be used for reinforcement in composite [1, 2] or biosensing [3]. Many biosensing devices have become a reality, especially

in biochemical sensing. The aim of the device is “to produce a signal that is proportional to the concentration of a chemical or biochemical to which the biological element reacts” [4]. Recently, Gholamzadeh and Nobovati [5] listed the many applications and various concepts behind the use of optical fibers for sensing, in a review on “fiber optic sensor”.

Glasses 45S5 and S53P4 have been developed by Hench [6] and Andersson et al. [7] respectively. These glasses are known to be highly bioactive and hence to form at their surface a hydroxycarbonated apatite (HCA) layer similar than the mineral part of bone [7, 8]. However, recent studies have shown that hot working of these glasses, such as drawing them into fibers, is difficult due to the rapid crystallization of these glasses at viscosity close to the sintering and/or drawing temperature [9]. Thus, the need for new glass compositions for the development of novel biomedical glass fibers becomes of great interest.

Phosphate glasses have been found to be good alternatives to silicate glasses as they are also suitable glasses for biomedical purposes, such as for example bone repair and reconstruction [10]. Even more, it is well known that the composition of the phosphate glasses can be tailored so these glasses can possess a low melting temperature, high dopant concentration, such as rare earth for example [11] or in general metals ions [12]. However, phosphate glasses are also known to have a fast dissolution rate limiting their application as biomedical glasses [13]. An in-depth dissolution study on phosphate glasses, conducted by Bunker et al. showed that the glass dissolution can be tailored and can even present dissolution rate similar to silicate glasses [14, 15].

From a biomedical point of view, SrO is naturally present in the human body [16] and Sr can easily replace Ca in the mineral part of the bone [17]. Studies have shown

J. Massera (✉) · M. Hupa · L. Hupa
Process Chemistry Centre, Åbo Akademi University,
Biskopsgatan 8, 20500 Turku, Finland
e-mail: jmassera@abo.fi

L. Petit · T. Cardinal · J. J. Videau
Institut de Chimie de la Matière Condensée de Bordeaux,
CNRS-Université Bordeaux 1, 87 Av. Dr. Schweitzer,
33608 Pessac, France

L. Petit
nLight Corporation, Sorronrinne 9, 08500 Lohja, Finland

that Sr can have a positive impact on preventing caries [18] and it is the only element which has been correlated to an increase in bone compression strength [16]. In phosphate glass, Sr and Ca have similar coordination number and are both glass modifiers; hence their role in the glass structure is expected to be similar [19].

In this paper, we present a study on the effect of Sr substitution for Ca on the thermal and structural properties of phosphate glasses. Thermal properties were measured using a differential thermal analyzer (DTA) and structural properties via ATR measurement. The glasses' reactivity in simulated body fluid (SBF) was, also, assessed. The pH of the SBF solution was measured every 2–3 days for 21 days. After 48, 168 and 504 h, glass particles were removed from the solution, rinsed and dried for ATR and SEM/EDXA analysis. Ions concentration in solution was measured via ICP-OES.

2 Experimental procedure

2.1 Glass processing

The glass samples were elaborated using standard melting method in platinum crucible. NaPO_3 , SrCO_3 , CaCO_3 and $(\text{NH}_4)_2\text{HPO}_4$ were used as raw materials. $\text{Ca}(\text{PO}_3)_2$ and $\text{Sr}(\text{PO}_3)_2$ precursors were first independently prepared using slow heating rate up to 900 °C. The precursors were mixed in the platinum crucible with the appropriate amount depending on the glass composition and melted at temperature ranging from 1,000 to 1,150 °C depending on the glass composition. The melt was poured on a brass mold and the resulting glass was annealed at 40 °C below the glass transition temperature.

2.2 Thermal properties

The glass transition temperature, T_g , and the crystallization temperature, T_p of the glasses were determined by differential thermal analysis (TGA/SDTA using a Mettler Toledo TGA/SDTA851°) at a heating rate of 10 °C/min on glass particle size ranging from 300 to 500 μm . The measurements were performed on 40–50 mg samples in platinum pans in an N_2 atmosphere. The glass transition temperature was taken at the inflection point of the endotherm, as obtained by taking the first derivative of the DTA curve. The crystallization temperature T_p was found at the maximum of the exothermic peak. From the thermogram, we can also measure T_{sol} and T_1 which are taken as the onset and endset of the melting (endothermic) peak, respectively. T_{sol} corresponds to the melting of the first crystal, while T_1 corresponds to the melting of the last crystal. The accuracy of the measurement is ± 3 °C.

2.3 Structural properties

The IR absorption spectra of the glasses were recorded using a Perkin Elmer FTIR in Attenuated Total Reflectance (ATR) mode on powdered glasses with grain size 300–500 μm . All IR spectra were recorded within the range 600–1,600 cm^{-1} and were corrected for Fresnel losses and normalized to the absorption band with maximum intensity.

The Raman spectra were recorded between 400 and 1,500 cm^{-1} at room temperature with a confocal micro-Raman Labram (Horiba/Jobin–Yvon) spectrometer in backscattering mode. The excitation source was a 532 nm continuous laser ($P_{\text{avg}} = 5.5$ mW). A holographic Notch filter was used to reject the Rayleigh diffusion. The backscattered light was collected through a 100 \times objective and selectively transmitted through the Notch filter towards a cooled CCD detector. The spectral resolution is 2 cm^{-1} .

2.4 “In vitro” reactivity

Powdered glasses with a grain size of 300–500 μm were immersed in SBF for up to 512 h at 37 °C in an incubating shaker (Stuart SI500) with an orbital speed of 120 rpm. SBF solution, developed by Kokubo et al. [20] was prepared following the methodology from the standard ISO/FDIS 23317. The change in the pH of the solution was recorded for various immersion times, using a pH/ion analyzer (Mettler Toledo MA235), and compared to a blank sample containing only SBF.

After 48, 168 and 512 h of immersion, 10 ml of the SBF solution containing glassy powder was diluted in 90 ml of ultra-pure water for ICP-OES measurement and the glass powder was filtered, rinsed with acetone and dried, for SEM/EDXA and ATR characterization.

Inductively coupled plasma-optical emission spectrometer (ICP-OES; Optima 5300DV, Perkin Elmer) was employed to quantify the amount of P, Sr, Ca and Na ions found in the SBF solution after glass immersion.

SEM/EDXA (Leo 1530 Gemini from Zeiss and EDXA from Vantage by Thermo Electron Corporation) was used to analyze the composition of the glassy powder and to evidence the formation of a layer after immersion in SBF. The accuracy of the elemental analysis is ~ 1.5 mol%.

3 Results

Figure 1 presents the DTA thermogram of the glasses with the composition $50\text{P}_2\text{O}_5-10\text{Na}_2\text{O}-(40-x)\text{CaO}-x\text{SrO}$ as a function x , measured at a heating rate of 10 °C/min. The position of the characteristic temperatures T_g , T_x , T_p , T_{sol} and T_1 are shown. Figure 2a exhibits T_g , T_x and T_p as a function of x . It is shown

that T_g , T_x and T_p decrease when x increases from 0 to 40 mol%. The decrease in T_g is more pronounced between $x = 0$ and 20 mol% while the decrease of T_p and T_x is more significant between $x = 20$ and 40 mol%. Figure 2b presents T_{sol} and T_l as a function of x . Both temperatures decrease when x increases from 0 to 20 mol% and then increase for

$x > 26.67$ mol% SrO. Using the values for T_g and T_x , ΔT ($\Delta T = T_x - T_g$) which is a gauge to the glass resistance toward crystallization [21], was calculated. Variation in ΔT as a function of SrO content is presented in Fig. 2c. ΔT first increases when x increases from 0 to 20 mol% and then decreases with a further increase in x . It is interesting to point out that all the investigated glasses exhibit a ΔT larger than 100 °C indicating that all glasses should have a good stability toward crystallization which is suitable for fiber drawing or hot working.

The structural properties of the glasses as a function of x were investigated using ATR and Raman spectroscopy. The IR spectra of the glasses are shown in Fig. 3a. All spectra were normalized to the band located at ~ 880 cm^{-1} . The spectra exhibit five absorption bands located around 1260, 1085, 880, 775 and 718 cm^{-1} and two shoulders at $\sim 1,154$ and 980 cm^{-1} . All bands shift towards lower wavenumbers with an increase in x . The bands at 1,260 and 1,085 cm^{-1} and the two shoulders at 1,154 and 980 cm^{-1} decrease in intensity, compared to that of the main band centered at 880 cm^{-1} whereas the intensity of the bands in the 650–800 cm^{-1} region increases when x increases.

Figure 3b presents the Raman spectra of the glasses. All spectra were normalized to the band with maximum intensity peaking at $\sim 1,175$ cm^{-1} . The spectra exhibit

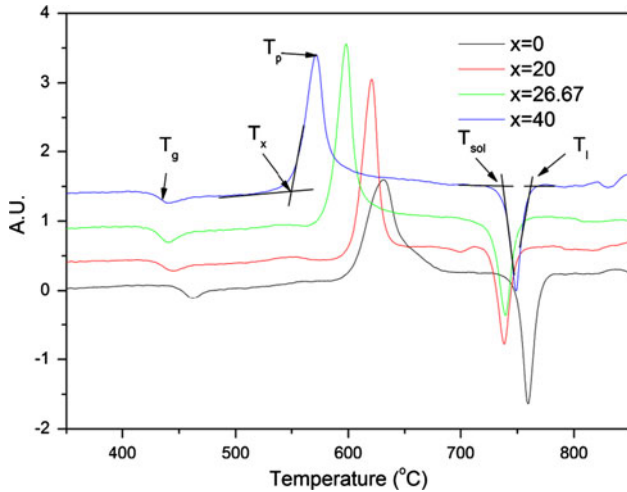


Fig. 1 DTA thermogram of the investigated glasses, as a function of x

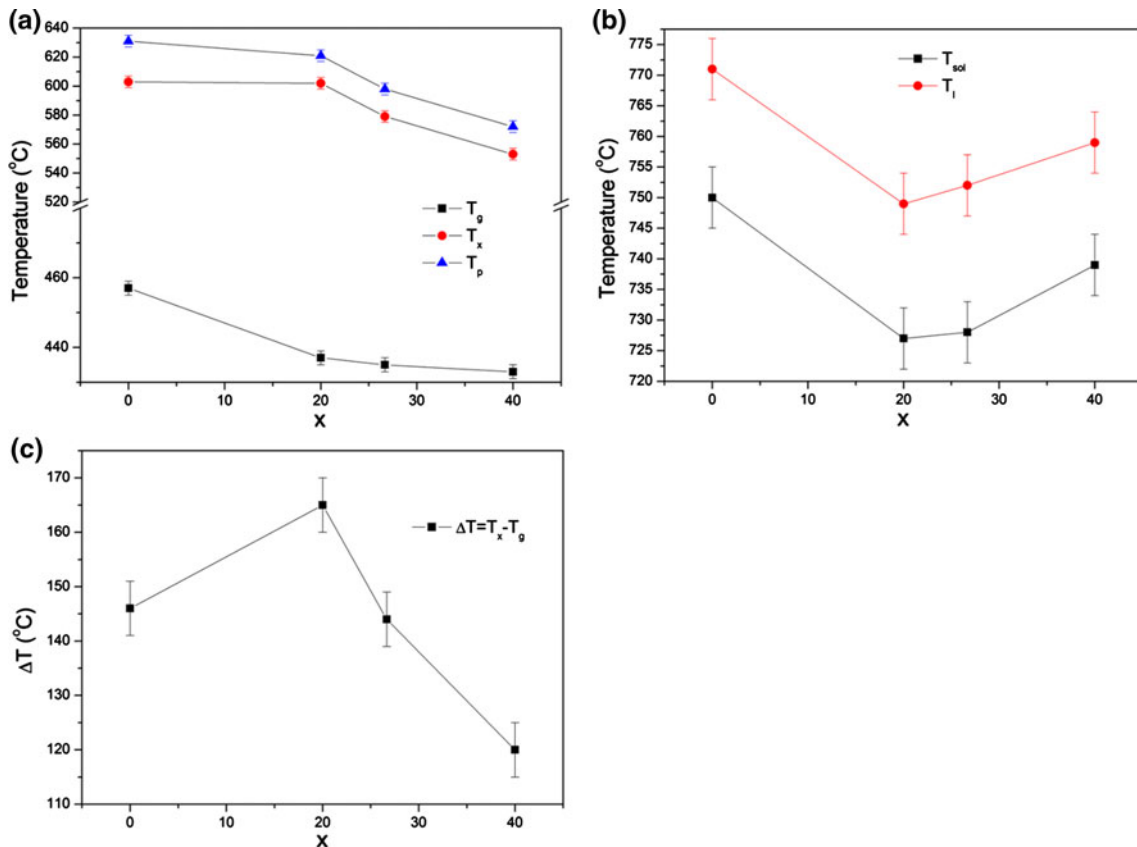


Fig. 2 Plot of T_g , T_x and T_p (a) T_{sol} and T_l (b) and ΔT (c) as a function of x

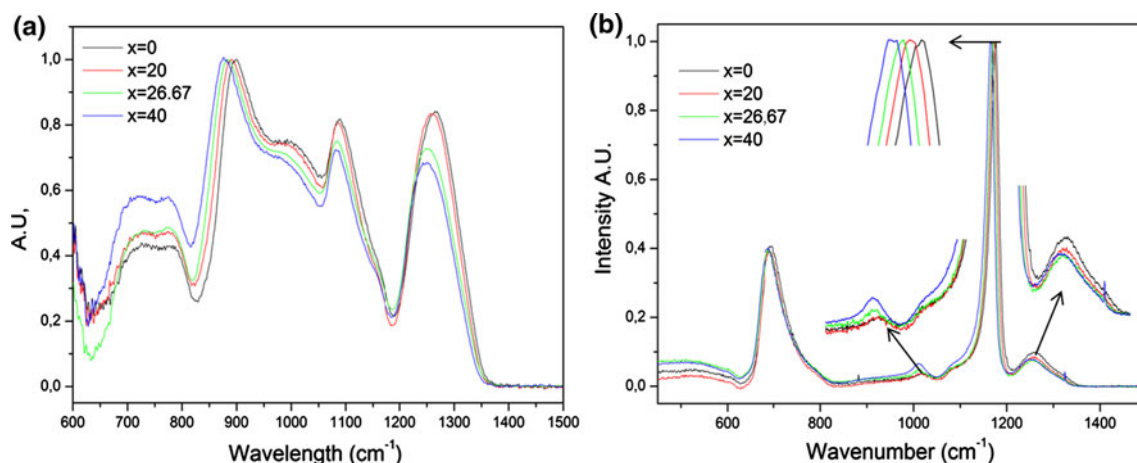


Fig. 3 IR (a) and Raman (b) spectra of the glasses

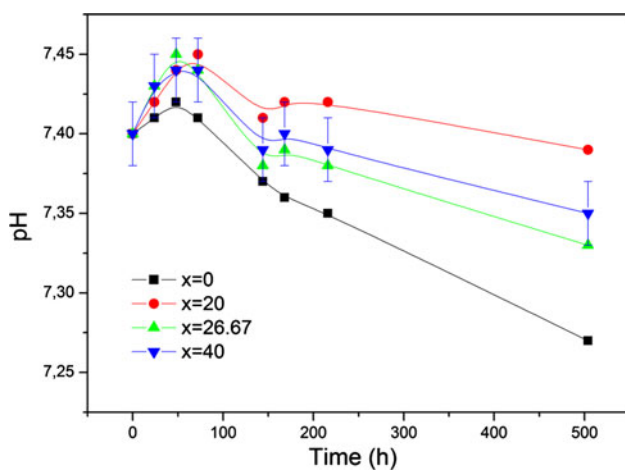


Fig. 4 pH of SBF solution as a function of immersion time

four bands and one shoulder. The bands located at ~ 1010 , 1175 and 1250 cm^{-1} , along with the shoulder at $1,095\text{ cm}^{-1}$ appear to shift to lower wavenumber. The band centered at $1,250\text{ cm}^{-1}$ exhibits a slight decrease in intensity whereas the bands at $1,010$ and $1,095$ increases in intensity with the progressive replacement of SrO for CaO compared to that of the band at $1,175\text{ cm}^{-1}$. The band at 690 cm^{-1} does not present any significant shift or change in intensity with the progressive increase in x .

Glass powder of each composition was immersed in SBF for 21 days. After 2 days of immersion, we observed a thin layer forming at the surface of the glasses, on all samples. The pH of the solution was measured every 2–3 days. Figure 4 presents the changes in pH as a function of the immersion time for the investigated samples. For all samples, the pH increases during the first 48 h of immersion and then decreases for longer immersion. The solution containing the glasses with $x = 0$ and 20 mol% were found to give rise to the highest and lowest decrease in pH, respectively.

Figures 5a–c show the evolution of the concentration in P, Ca and Sr, respectively, measured in the SBF solution as a function of immersion time and x . As seen in Fig. 5a, the P ions content in the SBF solution increases for all glasses as a function of immersion time. However, while the glass $x = 0$ exhibits the highest increase in P ions content in the solution, the glass with $x = 20$ mol% presents the least amount of P ions in solution at the end of the experiment ($t = 504\text{ h}$). As shown in Fig. 5b, the concentration of Ca ions in the SBF solution containing the glasses with $x = 0$ and 20 mol% first slightly increases during the first 48 h and then decreases when the immersion duration is increased to 168 h to finally remain constant for longer immersion time up to 500 h. The Ca ions content in the solution of the glasses with $x = 26.67$ and 40 mol% remains constant during the first 48 h of immersion and then progressively decreases for longer immersion time. It is important to remind that a decrease of the Ca ions content in the solutions indicates that Ca ions are consumed when the glasses are immersed in SBF. The concentration of Sr ions in solution, presented in Fig. 5c, increases with increasing immersion time and with increasing x . As expected from the composition of the glasses, a larger amount of Sr ions is found in the solution of the glass containing the highest SrO content ($x = 40\text{ mol}\%$).

After 48, 168 and 504 h of immersion, the glass particles were dried, embedded in resin and then polished to examine their cross section. Figure 6a, b present the SEM images of glass particles with $x = 0$ after 48 and 504 h of immersion, respectively. Figure 6c, d show the SEM images of glass particles with $x = 20\text{ mol}\%$ after 48 and 504 h of immersion, respectively. After 48 h of immersion in SBF, all glasses were found to have a layer forming at the surface of the glass particles, the thickness of which increases with an increase of the immersion duration independently of the glass composition (x). As seen in the

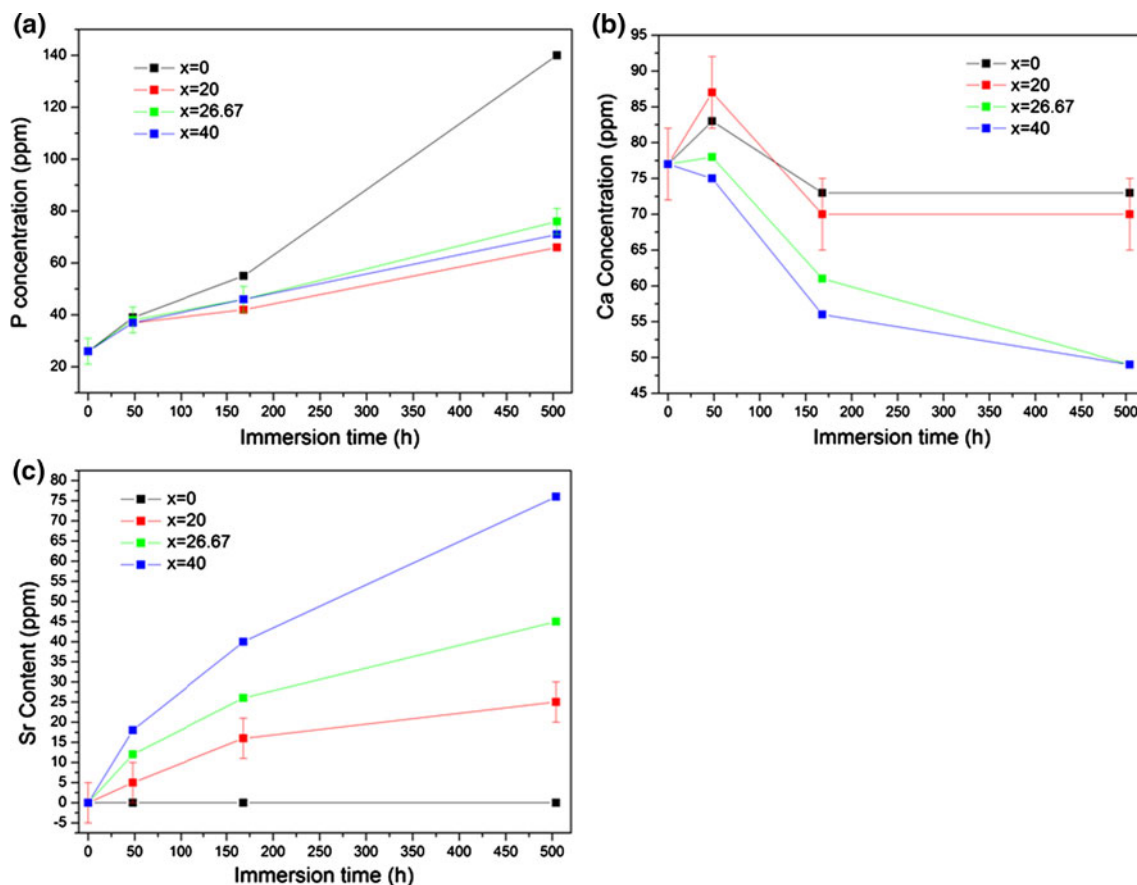


Fig. 5 Ions concentration in the SBF solution for P (a), Ca (b) and Sr (c) as a function of immersion time

Fig. 6, the layer thickness is $\sim 2\text{--}5\ \mu\text{m}$ after 48 h in SBF and increases to $20\text{--}35\ \mu\text{m}$ after 504 h of immersion. The composition of the layer and of the remaining glass was estimated using SEM/EDXA. Independently of the immersion duration, the glass composition was found to remain unchanged for all investigated samples. The layer composition as a function of the immersion time and composition is reported in Table 1. For all the glasses, the layer is formed by a lower concentration of Na_2O , P_2O_5 and SrO and a higher concentration of CaO . While the layers in all the investigated glasses have similar concentration of P_2O_5 (within the accuracy of the measurement), they have different CaO concentration and most probably different Na_2O content, the concentration of which decreases as x increases. Moreover, we noticed also an increase in the concentration of SrO in the layer as x increases. MgO was also found in the layer, the concentration of which increases with an increase of x . As seen in Table 1, with increasing immersion time, the concentration of P_2O_5 slightly decreases, the SrO and MgO content increases and we suspect a slight reduction in the Na_2O content. Within the accuracy of the measurement, the amount of CaO in the layer of the glasses with $x = 0$ and

20 mol% is suspected not to change significantly with increasing immersion duration whereas it decreases significantly in the layer forming at the surface of the glasses with $x = 26.67$ and 40 mol%.

Figure 7 presents the IR spectra of the glass with $x = 0$ (taken as an example), as a function of immersion time in SBF. With increasing the immersion time, the bands at $\sim 1,250$ and $\sim 780\ \text{cm}^{-1}$ progressively decreases in intensity whereas the amplitude of the band at $\sim 1,085\ \text{cm}^{-1}$ increases compared to that of the band at $880\ \text{cm}^{-1}$. Moreover, we can also notice that the shoulder at $980\ \text{cm}^{-1}$ disappears and a new band appears at $1,030\ \text{cm}^{-1}$, the intensity of which increases with an increase of the immersion time. All the investigated glasses were found to exhibit similar changes as a function of immersion time.

4 Discussion

In this paper, new phosphate glasses in the $50\text{P}_2\text{O}_5\text{--}10\text{Na}_2\text{O}\text{--}(40\text{--}x)\text{CaO}\text{--}x\text{SrO}$ glass system have been prepared in order to understand the impact of the replacement of Ca ions for Sr ions on the thermal and structural

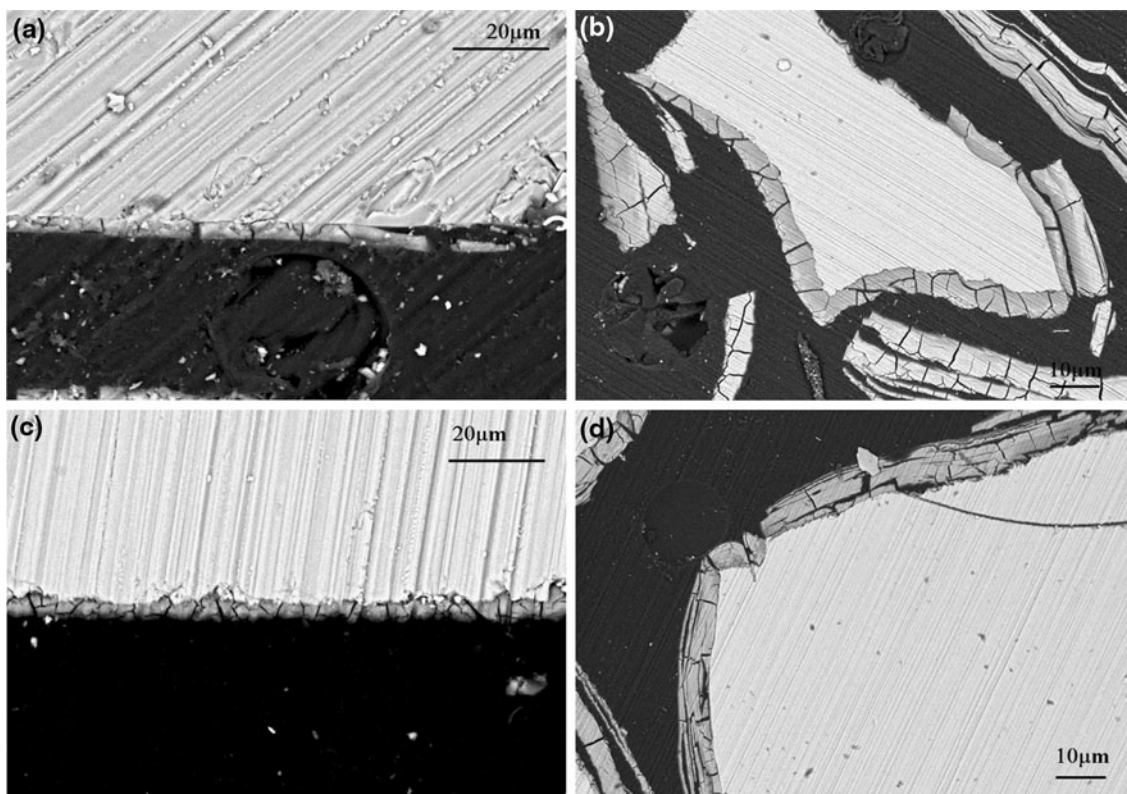


Fig. 6 SEM photographs of glass particles with $x = 0$ immersed in SBF for 48 h (a) and 504 h (b) and of glass particles with $x = 20$ mol% immersed in SBF for 48 h (c) and 504 h (d)

Table 1 Layer composition as a function of immersion time and x

Duration of immersion (h)	P ₂ O ₅ (mol%)	Na ₂ O (mol%)	CaO (mol%)	SrO (mol%)	MgO (mol%)
50P ₂ O ₅ –10Na ₂ O–40CaO ($x = 0$)					
48	37.9	4.2	53.3		4.6
168	36.9	3.8	53.6		5.7
504	34.6	3.2	55.1		7.1
50P ₂ O ₅ –10Na ₂ O–20CaO–20SrO ($x = 20$ mol%)					
48	36.3	3.8	50.9	3.4	5.5
168	34.7	2.6	50.3	4.8	7.5
504	33.2	2.3	49.6	6.6	8.3
50P ₂ O ₅ –10Na ₂ O–13.3CaO–26.7SrO ($x = 26.67$)					
48	37.6	3.9	47.1	4.9	6.5
168	35.2	2.1	47.1	7.7	7.9
504	33.6	2.8	43.6	10.5	9.5
50P ₂ O ₅ –10Na ₂ O–40SrO ($x = 40$ mol%)					
48	38.1	3.3	43.3	9.9	5.3
168	34.9	3.0	42.2	10.1	9.8
504	35.3	2.3	35.9	15.8	10.7

properties of the glasses. We also investigated its impact on the glass reactivity in SBF to check if these glasses can be considered good candidates as novel bioactive materials.

4.1 Thermal and structural properties

The thermal properties of the glasses are presented in Fig. 2. As seen in Fig. 2a, the replacement of Ca by Sr in

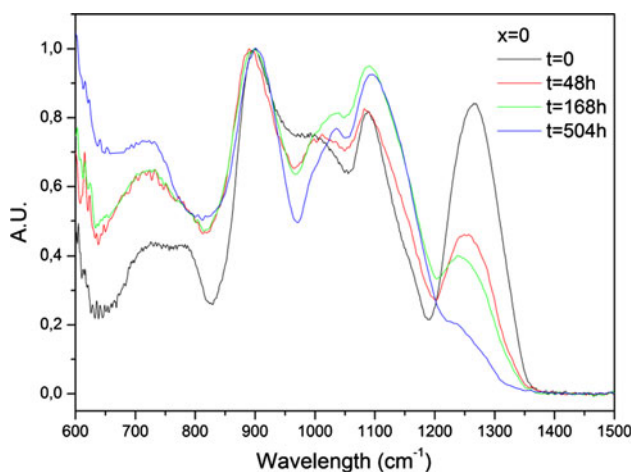


Fig. 7 IR spectra the glass with $x = 0$ as a function of immersion time

the phosphate glass leads to the formation of a glass with a lower T_g and T_p . This decrease in T_g and T_p can be attributed to a distortion of the glass network, due to the slightly larger size of Sr ions as compared to Ca ions. This is in agreement with [22, 23] who attributed the decrease in the glass transition (T_g) and crystallization temperatures to the formation of a less rigidly cross-linked glass network when Sr ions was substituted for Ca ions in silicate and phosphate glasses [22]. Similar changes in the glass transition and crystallization temperatures were observed when Ca ions were replaced by Sr ions in the well-known 45S5 glass [24]. ΔT , which is a gauge to the resistance to crystallization, is shown in Fig. 2c. ΔT first increases when x increases from 0 to 20 mol% and then decreases when x further increases to 40 mol%. It is interesting to notice that all glasses exhibit a ΔT larger than 100 °C, indicating that these glasses possess reasonable glass stability and can probably be drawn into fiber from preform without undesired crystallization. Hence, the SrO substitution for CaO up to $x = 20$ mol% appears to be the most beneficial glass composition for fiber drawing due to its highest ΔT . Moreover, one can notice, from Fig. 1, that the difference in temperature between the end of the crystallization peak and the beginning of melting increases with increasing the SrO content indicating that the addition of SrO at the expense of CaO in the investigated phosphate glass system appears to be also beneficial for drawing fibers from liquid. Especially, as shown in Fig. 2b, glasses with $x = 20$ and 26.67 mol% are of particular interest as their liquidus temperature occur at lower temperature.

The structure of the glasses was investigated using ATR and Raman spectroscopy. Figure 3a presents the IR spectra of the investigated glasses. All the absorption bands in the spectra can be attributed to the phosphate glass network. The main band at ~ 880 cm^{-1} is attributed to P–O–P asymmetric stretching of bridging oxygen in Q^2 units

(ν_{as} P–O–P Q^2) [25–27]. The shoulder centered at ~ 980 cm^{-1} and the band peaking at 1,085 cm^{-1} correspond to the symmetric and asymmetric stretching vibration of PO_3^{2-} in Q^1 units, respectively, [26, 28]. The band at 1,085 cm^{-1} can be attributed to an overlap between PO_3 Q^1 terminal group and PO_2 Q^2 groups in metaphosphate [29]. The shoulder at 1,154 cm^{-1} and the absorption band at 1,260 cm^{-1} correspond to symmetric and asymmetric vibration of PO_2^{2-} in Q^2 units, respectively [26, 28]. The absorption band located at 718 and 775 cm^{-1} are characteristic of P–O–P symmetric stretching vibration in metaphosphate structure [29]. The Raman spectra, in Fig. 3b, show four main bands at around 690 cm^{-1} corresponding to symmetric vibration P–O–P in metaphosphate type chains, 1,010 cm^{-1} attributed to symmetric stretch mode of NBO in Q^1 units, and at 1,175 and 1,250 cm^{-1} corresponding respectively to symmetric and antisymmetric vibrations of PO_2 also in phosphate chains [30–32]. The shoulder at $\sim 1,095$ cm^{-1} corresponds to motion of terminal oxygen bond vibration in phosphate chains [33]. From the Raman and IR spectra, we can conclude that the glass network of the investigated glasses is mainly formed of phosphate chains (metaphosphate type glass structure) with the presence of P–O–P entities formed with PO_2 units. The shift of the vibrations bands to lower wavenumber in the IR and Raman spectra is clearly observed when the calcium is replaced for the strontium. Such evolution can be related to a slight weakening of the P–O bonds. The slight weakening of the P–O bond can be attributed to the increase in the P–O–P bond angle in PO_4 tetrahedra as the field strength of Sr^{2+} is lower than Ca^{2+} [25]. From the Raman spectra, it is possible to believe that the strontium ion-containing glasses have slightly more Q^1 units than the SrO-free glass as evidenced by the slight increase in the intensity of the band located at 1,010 cm^{-1} and the decrease in the intensity of the band at 1,250 cm^{-1} in Fig. 3b. This is further confirmed with the decrease in the intensity of the band located at 1,260 cm^{-1} compared to the band at 1,085 cm^{-1} in Fig. 3a. This may indicate that the progressive introduction of SrO at the expense of CaO in the phosphate network leads to a more depolymerized phosphate chains.

4.2 Glass' reactivity in SBF

Powdered glasses with a grain size of 300–500 μm were immersed in SBF up to 512 h at 37 °C in an incubating shaker in order to compare the glass reactivity in SBF as a function of x .

As seen in Fig. 4, the pH of the solutions increases during the first 48 h but then decreases for longer immersion duration. The initial increase in the solution's pH can be attributed to the release of Na^+ , Ca^{2+} and/or Sr^{2+} ions

in solution as supported in Fig. 5, and as seen in [34]. For longer immersion time, the decrease of the pH, seen in Fig. 4, can be related to the change in P content in the SBF solution (Fig. 5a) [35] and so to the release of HPO_4 and PO_4^{3-} ions. As seen in Fig. 5, the glass with $x = 0$ when immersed in SBF releases the largest amount of P ions and consumes the less Ca, leading to a dramatic decrease in the solution pH. On the other hand, the strontium ion-containing glasses release a low amount of P ions but consume a large amount of Ca due to their low CaO content which leads to a small variation in the solution pH. One can notice that an increase of the SrO content in the phosphate glass leads to a larger consumption of Ca and also to a larger release of Sr in the solution. The consumption of Ca from the solution seen in Fig. 5a indicates that an apatite-like layer is progressively formed at the surface of the glass when it is immersed in SBF as seen at the surface of phosphate glasses with composition $44.5\text{P}_2\text{O}_5$ – 44.5CaO – $11\text{Na}_2\text{O}$ when immersed in SBF [10].

In order to confirm the formation of an apatite layer at the surface of the glasses, the structure of the glasses were analyzed with ATR after 48, 168 and 504 h of immersion in SBF. Figure 7 presents the IR spectra measured at the surface of the SrO-free glass particles as a function of immersion time in SBF. With increasing the immersion time, the absorption band at $1,250\text{ cm}^{-1}$ and the shoulder at $1,154\text{ cm}^{-1}$ decrease in intensity indicating that the amount of Q^2 units decreases. Moreover, the absorption band at $1,085\text{ cm}^{-1}$ increases in intensity indicating an increase in the Q^1 units. These changes in the spectra can be attributed to the depolymerization of the glass due to an hydration of the phosphate chains as reported in [10]. More importantly, a new band at $1,030\text{ cm}^{-1}$ appears with increasing the immersion time. This band can be attributed to PO^- in Q^0 units which are characteristics of orthophosphate groups as seen in [36] and could correspond to an apatitic like configuration. One can also observe a decrease in intensity of the band at 775 cm^{-1} and an increase in intensity of the band at 715 cm^{-1} revealing a decrease in bond length and/or the formation of orthophosphate groups when the glass is in contact with SBF. The same changes were observed in the spectra of the other glasses.

As the change in the solution pH can be related to the glass dissolution rate [37], the Sr-free glass is expected to have higher dissolution rate than the strontium ion-containing glasses. Based on our former work [15] and also on [14], the dissolution rate of a glass depends on its network dimensionality. It is expected to increase when lowering the cross-linking of the glass network. Based on the analysis of the IR spectra, the addition of SrO at the expense of CaO should lead to an increase in the dissolution rate which is in disagreement with the evolution of the solution

pH as a function of immersion duration seen in Fig. 4. In order to understand this, the composition of the remaining glass and of the apatite layer was checked using SEM/EDXA. Independently of the immersion time, no variation in the composition within the accuracy of measurement was observed for the remaining glasses confirming that the investigated glasses dissolve uniformly in SBF as discussed in [14]. The composition of the formed layer is reported in Table 1. P, Na, Ca, Sr and Mg ions were found in the layer. The P_2O_5 content in the layer decreases with increasing the immersion time which is in agreement with the increase of the P content in the SBF solution (Fig. 5) and also with the formation of an apatite type layer. The CaO content decreases whereas the SrO content increases in the layer with increasing x . This is due to the fact that when SrO is substituted for CaO in the glass, less Ca^{2+} ions are available for the layer formation leading to a higher Ca consumption from the liquid, as seen in Fig. 5. Even more, the concentration of MgO in the layer increases with increasing x . Mg ions come from the SBF solution and are likely introduced in the apatitic layer during its formation. Indeed it is well known that Mg and Sr ions can substitute Ca ions in an apatite layer [38]. We think it is because of the presence of SrO and MgO in the layer, that the glass with $x = 20\text{ mol}\%$ exhibits a lower variation in the solution pH when in contact with SBF than the glass with $x = 0$ while these glasses have a similar structure as seen in Fig. 3. The larger solution pH reduction when x increases from 20 to 40 mol% SrO might be related to the structure of the glasses. As explained in the previous paragraph, the replacement of Ca ions by Sr ions leads to the formation of a glass network with lower bond strength and less cross-linked network and so a glass with a slightly higher dissolution rate. It should be noted that the decrease in phosphate leaching from the SrO-containing glasses does not seem to impair the formation of the apatite layer. This can be attributed to the presence of the Sr ions in the apatitic layer and/or in the solution. Indeed it has been reported that Sr ions increase the nucleation of apatite crystals [38, 39].

5 Conclusion

The effect of Ca ions replacement by Sr on the thermal property and surface reactivity of phosphate glasses has been investigated in order to engineer new glass candidates for biomedical glass fibers. From the analysis of the thermal properties, we showed that the substitution of SrO for CaO leads to glasses with better thermal stability upon crystallization and a wider temperature window between the end of the crystallization peak and the beginning of melting, indicating that the strontium ion-containing

glasses might be suitable for fiber drawing from preform and, also, from liquid. From a glass surface reactivity point of view, when immersed in SBF, all glasses were found to precipitate an apatite-like layer, the thickness of which increases with increasing the immersion time independently of the glass composition. The formation of the apatite-like layer was confirmed using ATR. During the layer formation, the amount of phosphate ions released in solution as a function of immersion time was found to be less for the SrO-containing glasses which leads to less change in pH. Using SEM/EDXA, Na₂O, P₂O₅, SrO, CaO and MgO were found in the apatite layer of the strontium ion-containing glasses. The concentration of SrO and MgO was found to increase with an increase of SrO content. We think it is the presence of SrO and MgO in the apatite layer which plays an important role in the limitation of phosphate leaching in the solution and so of the glass dissolution. All glasses were found to form an apatitic layer regardless of the phosphate leaching limitation. This is probably due to the Sr ions incorporation in the apatitic layer and/or in solution. The reduced change in the solution pH with respect to immersion times along with improved thermal properties makes the strontium ion-containing phosphate-based glasses promising glasses as bioactive glass fibers.

Acknowledgment We acknowledge the support of the Åbo Akademi Foundation and the National Center of Excellence Program by the Academy of Finland. The Academy of Finland is gratefully acknowledged for the financial support of the author (J.M.).

References

1. Marcolongo M, Ducheyne P, Lacourse WC. Surface reaction layer formation in vitro on a bioactive glass fiber/polymeric composite. *J Biomed Mater Res*. 1997;37:440–8.
2. Pirhonen E, Törmälä P. Coating of bioactive glass 13–93 fibres with biomedical polymers. *J Mater Sci*. 2006;41:2031–6.
3. Clupper DC, Hall MM, Gough JE, Hench LL. S520 and 45S5 glass fibers: bioactivity, mechanical properties, and osteoblast attachment. Tampa: Transactions of the Society for Biomaterials; 2002.
4. Bosch ME, Sanchez AJR, Rojas FS, Ojeda CB. Review: recent development in optical fiber biosensors. *Sensors*. 2007;7:797–859.
5. Gholamzadeh B, Nobovati H. World of academy of science, engineering and technology, vol 42. New York: Fiber Optic Sensor; 2008. p. 297–307.
6. Hench LL, Andersson ÖH. Bioactive glasses. In: An introduction to bioceramics. June Wilson; 1993.
7. Andersson ÖH, Karlsson KH. Corrosion of bioactive glass under various in vitro conditions. *Advance in Biomaterials No 8*. Amsterdam: Elsevier; 1990.
8. Cao W, Hench LL. Bioactive materials. *Ceram Int*. 1996;22:493–507.
9. Massera J, Fagerlund S, Hupa L, Hupa M. Crystallization behavior of the commercial bioactive glasses 45S5 and S53P4. *J Am Ceram Soc*. 2012;95:607–13.
10. Clement J, Manero JM, Planell JA. Analysis of the structural changes of a phosphate glass during its dissolution in simulated body fluid. *J Mater Sci Mater Med*. 1999;10:729–32.
11. Gapontsev VP, Matitsin SM, Isineev AA, Kravchenko VB. Erbium glass lasers and their applications. *Opt Laser Technol*. 1982;14:189–96.
12. Ahmed AA, Ali AA, Mahmoud DAR, El-Fiqi AM. Preparation and characterization of antibacterial P₂O₅–CaO–Na₂O–Ag₂O glasses. *J Biomed Mater Res A*. 2011;98:132–42.
13. Salih V, Franks K, James M, Hastings GW, Knowles JC, Olsen I. Development of soluble glasses for biomedical use part II: the biological response of human osteoblast cell lines to phosphate-based soluble glasses. *J Mater Med*. 2000;11:615–20.
14. Bunker BC, Arnold GW, Wilder JA. Phosphate glass dissolution in aqueous solutions. *J Non Cryst Solids*. 1984;64:291–316.
15. Massera J, Bourhis K, Petit L, Couzi M, Hupa L, Hupa M, Videau JJ, Cardinal T. Study of the chemical durability of phosphate-based glasses in different solutions. *J Phys Chem Solids*. 2013;74:121–7.
16. Isaac J, Nohra J, Lao J, Jallot E, Nedelec J-M, Berald A, Sautier J-M. Effects of strontium-doped bioactive glass on the differentiation of cultured osteogenic cells. *Eur Cells Mater*. 2011;21:130–43.
17. Vaughan J. The physiology of bone. 3rd ed. Oxford: Clarendon Press; 1981.
18. Curzon ME. The relation between caries prevalence and strontium concentrations in drinking water, plaque, and surface enamel. *J Dent Res*. 1985;64:1386–8.
19. Toyoda S, Fujino S, Morinaga K. Density, viscosity and surface tension of 50RO–50P2O5 (R: Mg, Ca, Sr, Ba, and Zn) glass melts. *J Non Cryst Solids*. 2003;321:169–74.
20. Kokubo T, Kushitani H, Sakka S, Kitsugi T, Yamamuro T. Solutions able to reproduce in vivo surface-structure changes in bioactive glass-ceramic A-W³. *J Biomed Mater Res*. 1990;24:721–34.
21. Dietzel A. Entstehung von Inhomogenitäten in der Glasschmelze durch Verdampfung einzelner Bestandteile. *Glasstech Berl*. 1957;30:134–8.
22. Fredholm YC, Karpukhina N, Law RV, Hill RG. Strontium containing bioactive glasses: Glass structure and physical properties. *J Non Cryst Solids*. 2010;356:2546–51.
23. Konidakis I, Varsamis C-PE, Kamitsos EI, Möncke D, Ehrh D. Structure and properties of mixed strontium-manganese metaphosphate glasses. *J Phys Chem*. 2010;114:9125–38.
24. Fujikura K, Karpukhina N, Kasuga T, Brauer DS, Hill RG, Law RV. Influence of strontium substitution on structure and crystallisation of Bioglass® 45S5. *J Mater Chem*. 2012;22:7395–402.
25. Shih P-Y, Shiu H-M. Properties and structural investigations of UV-transmitting vitreous strontium zinc metaphosphate. *Mater Chem Phys*. 2007;106:222–6.
26. GaO H, Tan T, Wang D. Effect of composition on the release kinetics of phosphate controlled release glasses in aqueous medium. *J Control Release*. 2004;96:21–8.
27. Moustafa YM, El-Egili K. Infrared spectra of sodium phosphate glasses. *J Non Cryst Solids*. 1998;240:144–53.
28. Neel EAA, Chrzanowski W, Pickup DM, O’Deel LA, Mordan NJ, Newport RJ, Smith ME, Knowles JC. Structure and properties of strontium-doped phosphate-based glasses. *J Royal Soc Interface*. 2009;6:435–46.
29. Ilieva D, Jivov B, Bogachev G, Petkov C, Penkov I, Dimitriev Y. Infrared and Raman spectra of Ga₂O₃–P₂O₅ glasses. *J Non Cryst Solids*. 2001;283:195–202.
30. Lee S, Obata A, Kasuga T. Ion release from SrO–CaO–TiO₂–P₂O₅ glasses in Tris buffer solution. *J Ceram Soc Jpn*. 2009;117:935–8.
31. Karakassides MA, Saranti A, Koutselas I. Preparation and structural study of binary phosphate glasses with high calcium and/or magnesium content. *J Non Cryst Solids*. 2004;347:69–79.

32. Kalampounias AG. Short-time vibrational dynamics of metaphosphate glasses. *J Phys Chem Solids*. 2012;73:148–53.
33. Ciceo Lucacel R, Hulpus AO, Simon V, Ardelean I. Structural characterization of phosphate glasses doped with silver. *J Non Cryst Solids*. 2009;355:425–429.
34. Rajkumar G, Rajkumar M, Rajendran V, Samickannian Aravindan S. Influence of Ag_2O in physico-chemical properties and HAp precipitation on phosphate-based glasses. *J Am Ceram Soc*. 2011;94:2918–25.
35. Ahmed I, Lewis M, Olsen I, Knowles JC. Phosphate glasses for tissue engineering: part 1. Processing and characterisation of a ternary-based P_2O_5 -CaO- Na_2O glass system. *Biomaterials*. 2004;25:491–9.
36. Manupriya M, Thind KS, Singh K, Sharma G, Rajendran V. Influence of addition of Al_2O_3 on physical, structural, acoustical and in-vitro bioactive properties of phosphate glasses. *Phys Status Solidi A*. 2009;206:1447–55.
37. Franks K, Abrahams I, Knowles JC. Development of soluble glasses for biomedical use part i: in vitro solubility measurement. *J Mater Sci Mater Med*. 2000;11:609–14.
38. Driessens FCM, Verbeeck RMH. *Biomaterials*. Boca Raton: CRC Press; 1990, pp. 86–89; 259–260.
39. Pan HB, Li ZY, Lam WM, Wong JC, Darvell BW, Luk KD, Lu WW. Solubility of strontium-substituted apatite by solid titration. *Acta Biomaterialia*. 2009;5:1678–85.